Chapter 2 Background

This chapter introduces some background relvent to the disscussion in this thesis. Section 2.1 is a summery of previous theoretical and experimental studies on exchange anisotropy. Section 2.2 presents the magnetic properties of IrMn.

2.1 Exchange anisotropy

2.1a Origin of the Exchange Anisotropy

When materials with ferromagnetic (FM) and antiferromagnetic (AFM) interfaces are cooled through the Neel temperature (T_N) of AFM (with the Curie temperature, T_C of FM larger than T_N) an exchange anisotropy (exchange bias) is induced in FM [1], and their characteristic signature are the shift of the center of hysteresis loops from their normal position at H=0 to H≠0. Exchange anisotropy was first discovered in 1956 by Meiklejohn and Bean [2]. Their discovery was initated by the observation that the hysteresis loop below room temperature of a sample of niminal Co nano particles was shifted along the field after cooling in an applied field. It was subsequently established that the particles could be considered to consist of a core of single-domain Co with a shell of AFM CoO. Fig. 2.1(a) shows the hysteresis loops at 77K of partially oxides Co particles. A shifted loop (curve 1) was obtained after cooling in the field of 10 KOe; the symmetric loop (curve 2) was obtained after cooling in zero field. In addition, according to

the result shown by torque magnetometry at $T<T_N$ after field cool, Fig. 2.1(b), a combination of $\sin^2\phi$ (uniaxial anisotropy) with a $\sin\phi$ component is performed, where ϕ is the angle between the applied field and the cooling field direction. Therefore, instead of purely uniaxial anisotropy, i.e. two equivalent easy configurations in opposite directions, the magnetization in FM/AFM systems has only one easy direction, often denoted as unidirectional anisotropy [3].

Since the first experiments of Meiklejohn and Bean, exchange anisotropy was observed in many FM/AFM systems such as small particles, inhomogeneous materials and thin films. A detailed review was shown in reference [4]. Recently, the exchange bias phenomenon has been of great interest to industry due to its application in spin valve devices [5] and magnetoresistive random access memory (MRAM) [6].

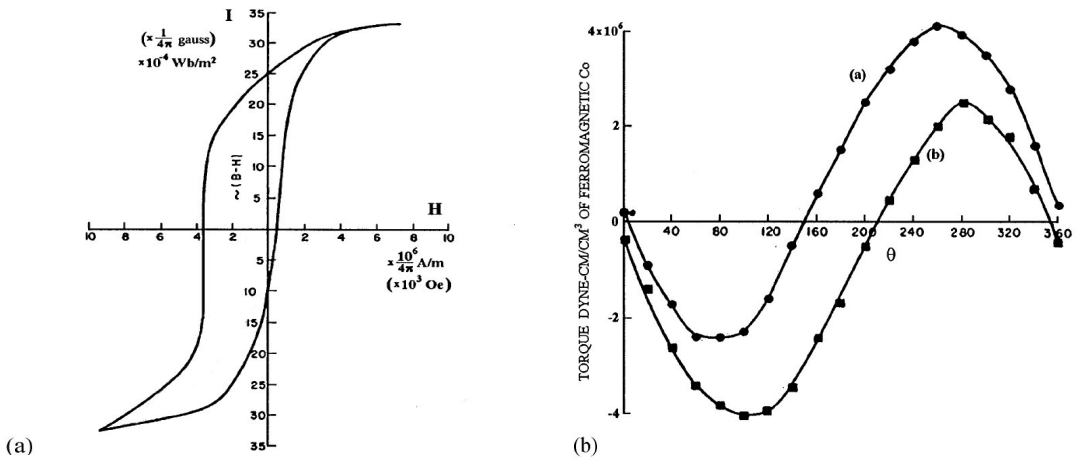

Fig. 2.1 (a) The hysteresis loop, and (b) the torque curves for the Co-CoO sample cooled in the field and measured at 77K. Curve a and b in (b) are for countercloclwise and clockwise rotations, respectively. The area between curve a and b is the rotational hysteresis loss. (Data are from Meiklejohn's study of Co/CoO [3])

2.1b Previous Experiments Reports

In addition to the symmetry breaking related to the appearance of the unidirectional anisotropy that brings about the exchange field, several supplementary remarkable features are associated with the exchange anisotropy, which have been listed below:

Blocking temperature (Tb)

At a critical temperature called “Blocking temperature”, the exchange field, which is equal to the shift of the hysteresis loops, decrease to zero. Usually T_B can be found to be lower than the Neel temperature (T_N) of coupled ferromagnetic. The thermal fluctuation model[7] enables us to understand quantitatively the dependence of the blocking temperature on the magnetic properties, such as the transition temperatures of the FM (T_C) and AFM (T_N), and structural properties, such as the grain size of AFM, shown in Fig 2.2, that is extend through the thickness, of the polycrystalline FM/AFM bilayers and on the hysteresis loop measurement time or frequency.

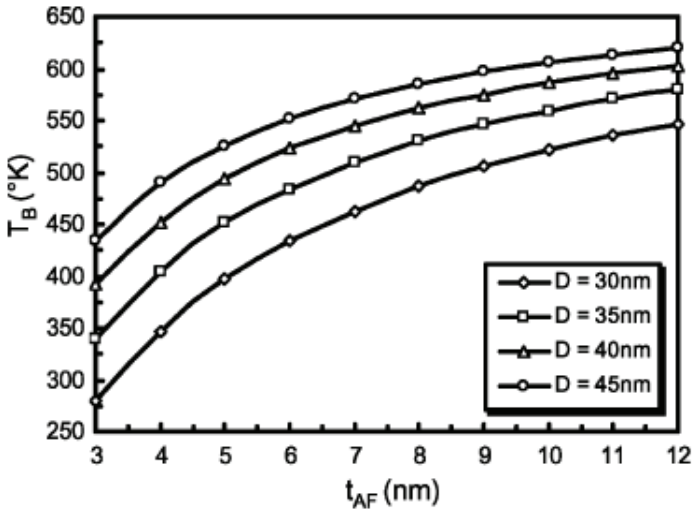

Fig. 2.2 AF thickness dependence of the blocking temperature for AF grain sizes of 30, 35, 40, and 45 nm [7].

Training Effect

In many exchange bias systems, a gradual degradation of exchange bias field (H_e) can be observed upon cycling the heterostructure through consecutive hysteresis loops, called training effect [8]. It is generally believed that this effect comes from irreversible changes such as reorientation of domain and spin configuration in the AFM layer with each FM magnetization reversal. An experimentally formula

$$\mu_0 H_e(n) - \mu_0 H_e^0 = \frac{\kappa}{\sqrt{n}} \qquad (2.1)$$

where n is the order of consecutive loops are measured; κ is system dependent constant and $\mu_0 H_e^0$ is the exchange bias field in the limit of infinite loops [9].

Asymmetric Reversal

One of the unusual properties related to the exchange bias effect is asymmetric magnetization reversal in both branches of a hysteresis loop, as observed in many FM/AFM system such as NiFe/FeMn [10], TMF_2/Fe (TM is transition metal) [11], NiFe/NiO [12], Co/IrMn [13]. To investigate this phenomenon, several experimental techniques have been taken to provide information on the magnetization reversal, such as domain imaging [14], polarized neutron reflectometry [15], anisotropic magnetoresistance [16],vectorial Kerr magnetometry [17], or vectorial susceptibility [18]. It has been observed that the magnetization reversal is different at each branch of the (shifted) hysteresis loop and this asymmetry depends on the angle between the external field and the exchange bias direction. Based on above experimental techniques, it is now understood that magnetization reversal occurs by domain wall motion on one side of the magnetic hysteresis loop and by magnetization rotation on the other side. The origin of the asymmetric reversal has been correlated with the existence of higher order FM anisotropies, dispersion of the FM or AFM anisotropy axes, or irreversibilities due to training.

2.1c Models for Exchange Anisotropy

2.1.c.1 Ideal Interface Model (1957)

The first simple model of exchange anisotropy proposed by Meikljohn and Bean [2] examined the situation of the FM and AFM layers are both single crystalline and epitaxial across an atomically smooth FM/AFM interface. Fig. 2.3 shows a fully uncompensated AFM interface layer, which has all of the spin direction in the same orientation as the neighboring FM layer. This results in an interface energy difference across the FM/AFM interface. During the reversal of the FM magnetization in this ideal model, the spins of the FM layer rotate coherently, while the spins of the AFM layer remained fixed. The energy cost is determined by balancing the Zeeman, magnetocrystalline anisotropy and exchange anisotropy energies. The general equation of total energy per unit area E (erg/cm^2) can be expressed as :

$$\mathbf{E= -H\bullet M_s t_{FM} + K_{FM} t_{FM} \sin^2\theta - K_e \cos\theta} \qquad \mathbf{(2.2)}$$

where **H** is the applied field; $\mathbf{t_{FM}}$ is the thickness of FM; $\mathbf{K_e}$ (erg/cm^2) is the exchange anisotropy and $\mathbf{K_{FM}}$ is the magnetocrystalline anisotropy of FM; **θ** is the angle between applied field and easy axis, respectively. Futhermore, by considering the switching field of FM with the magnetization changes from θ=0° to θ=180°, the first derivative of equation (2.2) is taken. The switching field can be expressed as:

$$\mathbf{H_{switching}=(2K_{FM}/M_s)+[K_e/M_s t_{FM}]} \qquad \mathbf{(2.3)}$$

The equation (2.3) shows a combination of the intrinsic switching field of FM (first term), and exchange field contributed by FM/AFM coupling (second term). Therefore, the exchange field is $\mathbf{H_e=K_e/M_s t_{FM}}$.

In order to estimate the K_e, taking the exchange energy per pair of FM/AFM atoms as $\mathbf{J_{ex}S_{FM}S_{AFM}}$. $\mathbf{J_{ex}}$ is the exchange paremeter; $\mathbf{S_{FM}}$ and $\mathbf{S_{AFM}}$ are the spins of the interfacial atoms. If there are N atoms at the interface and its area is **A**, the exchange anisotropy energy (K_e) can be expressed as $\mathbf{NJ_{ex}S_{FM}S_{AFM}/A}$. By substituting **N** to $\mathbf{A/a^2}$, which **a** is the atomic spacing, one could finally get:

$$\mathbf{K_e=2J_{ex}S_{AFM}S_{FM}/a^2} \qquad \mathbf{(2.4)}$$

and

$$\mathbf{H_e=K_e/M_{FM}t_F=}\ \frac{2J_{ex}S_{AFM}S_{FM}}{a^2 M_{FM} t_{FM}} \qquad \mathbf{(2.5)}$$

The major problems associated with this model are the prediction of exchange bias fields that are two orders of magnitude larger than the observed values, failure to explain the exchange biasing observed at fully compensated interfaces and not taking into account the existence of interface roughness which exists in sputtered polycrystalline thin films.

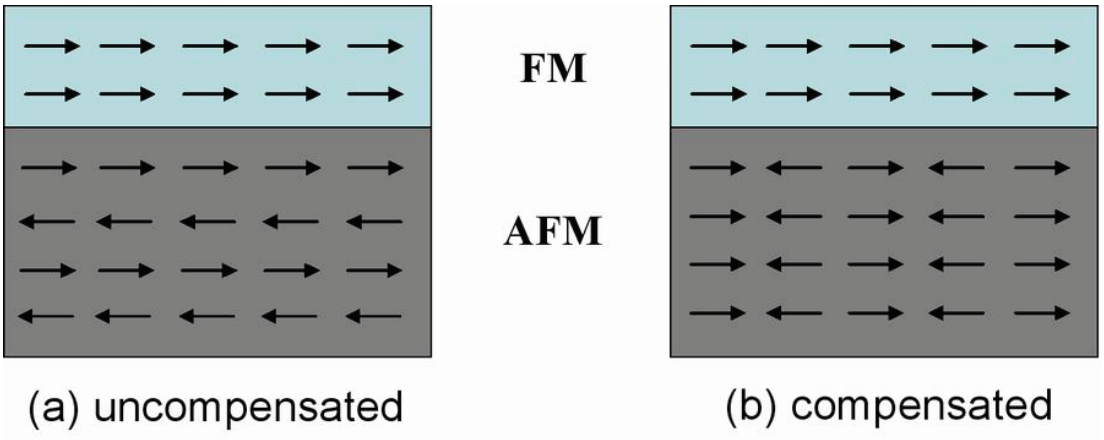

Fig. 2.3 Side view of AFM/FM interface showing the spin orientation in the (a) uncompensated and (b) the compensated state.

2.1.c.2 AFM domain wall model (1987)

To explain the discrepancy between the exchange field value predicted by equation **(2.5)** and experimental results. Mauri, et al. [19], proposed the existence of a planar domain wall parallel to the FM/AFM interface as a modification to ideal interface model. As shown in Fig. 2.4, the model successfully lowers the energy required for the magnetization reversal of FM layer. Based on several assumptions that : (i) an AFM domain can form at the FM/AFM interface; (ii) the thickness of FM is much smaller than the FM domain wall width; (iii) the AFM layer is infinitely thick so that there is no restrictions for the AFM domain wall formation.

With the magnetiztion reversal of the FM layer, the required energy per unit area would be equal to the $2\sqrt{K_{AFM} A_{AFM}}$, which is AFM domain wall

energy per unit area. Therefore, the model predicts that the exchange field is given by:

$$\mathbf{H_e} = 2\sqrt{K_{AFM} A_{AFM}} / \mathbf{M_{FM} t_{FM}} \quad \textbf{(2.6)}$$

And

$$\mathbf{K_e} = 2\sqrt{K_{AFM} A_{AFM}} \quad \textbf{(2.7)}$$

Where A_{AFM} is the exchange stiffness parameter and K_{AFM} is the magnetocrystalline anisotropy of the AFM layer. In this model, K_e is reduced by a factor of $\sqrt{K_{AFM} A_{AFM}}$ by spreading the energy over an entire domain wall rather than over an sharp interface, as in the ideal interface model.

However, this model does not explain the origin of exchange bias at compensated interfaces and persistence of exchange anisotropy without diminution of H_e down to an AFM thickness of 2.5nm, an order of magnitude lower than the characteristic AFM domain wall width. Although the AFM domain wall model does not explain completely for experimental results, it does introduce the important concept of domain formation in the AFM layer as a factor in determining the magnitude of the exchange bias effect.

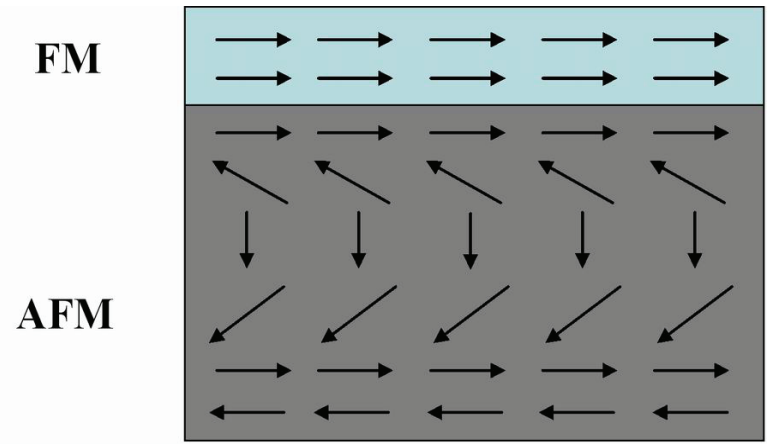

Fig. 2.4 Schematic diagram of spin configuration in the AFM domain wall model.

2.1.c.3 Random Field model (1987)

Malozemoff [20], explained the source of the exchange bias effect as originating from the imbalance in the interfacial spins at the AFM/FM interface caused by the interface roughness. The interface roughness results in frustrated bumps at the AFM/FM interface, as shown in Fig. 2.5(a) has high interfacial energy. The cross marks represent the frustrated bumps. The amount of the interfacial energy is reduced through the parallel arrangement of the spins in AFM interface layer to the FM layer as seen in Fig. 2.5(b). Consequently, the interfacial inhomogeneities create localized sites of unidirectional interfacial energy $\sigma_1=zJ/a^2$, where J is the interfacial exchange parameter, a is cubic lattice parameter, $\mathbf{z}$ is a number of order unity. Random field theory argues that a net average non-zero interfacial

energy will exist, particularly when the average is taken over a small number of sites. Statistically, the average σ in an area of L^2 will decrease as $\sigma \approx (\sigma_1/\sqrt{N})$ where $N=(L^2/a^2)$ is the number of sites projected onto the interface plane. Given the random and assuming a single domain FM film, the AFM film will divide into domain-like regions to minimize the net random unidirectional anisotropy.

Although expansion of the domain size *L* would lower the random field energy, in-plane uniaxial anisotropy energy K_{AF} in the AFM layer will limit the domain size. Anisotropy energy confines the domain wall width to $\pi\sqrt{K_{AFM} A_{AFM}}$ (<L), and creates an additional surface energy term of the domain wall $4\sqrt{K_{AFM} A_{AFM}}$ (surface tension in bubble domain). The balance between exchange and anisotropy energy is attained when $L \approx \pi\sqrt{K_{AFM} A_{AFM}}$. Therefore, the average interfacial exchange energy density K_e becomes:

$$K_e = 4zJ_{ex}/\pi aL \tag{2.8}$$

Where z is the number of order unity for the AFM. With $J_{ex} \approx A_{AFM}/a$ and $L \approx \pi\sqrt{K_{AFM} A_{AFM}}$, equilibrium domain size, H_e is changed to the following equation:

$$H_e = \frac{\Delta\sigma}{2 M_F t_F} = \frac{2z\sqrt{A_{AF}K_{AF}}}{\pi^2 M_F t_F} \tag{2.9}$$

The random-field model also explained the reduction in the exchange bias energy, but was only applied to case of a single crystal AFM layer. It did nothing to explain the situation in polycrystalline thin films where grain boundaries, vacancies, and other defects are present. The model has also never been experimentally confirmed. It did however introduce the concept of domain interaction in the AFM layer with defects in the AFM that would be central to later exchange bias models.

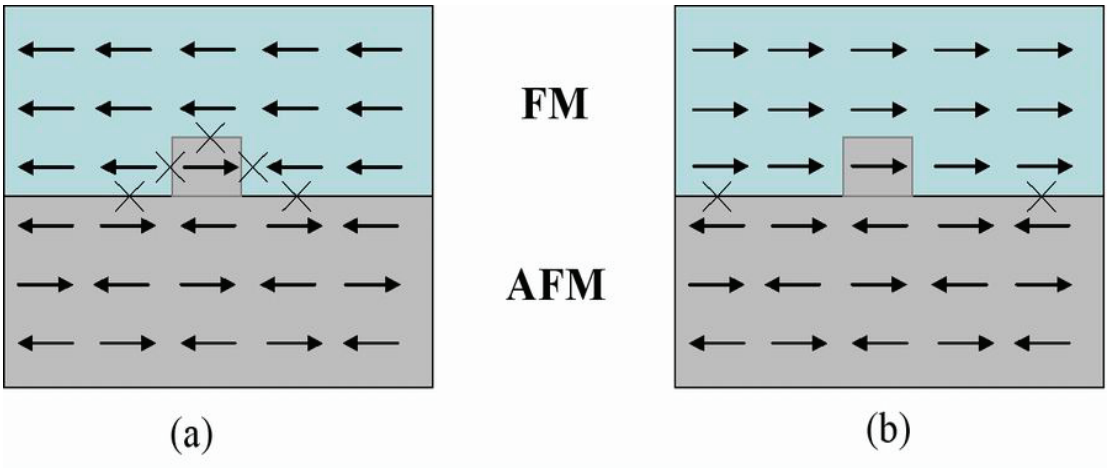

Fig. 2.5 Schematic diagrams of possible spin configuration in the random field model.

2.1.c.4 “Spin Flop” Perpendicular Interfacial Coupling (1997)

The “spin-flop” model introduced by Koon [21] is on the basis of micromagnetic numerical calculations. From the calculations indicate that in a fully compensated AFM interface, the stability of interfacial exchange coupling with a perpendicular orientation between the FM and AFM axes directions. He refers to the perpendicular interfacial coupling as “spin-flop” coupling. To observe perpendicular interfacial coupling, his model specifies the structure and orientation of the AFM layer as a single-crystal body centered tetragonal (BCT) structure, shown in Fig. 2.6(a). The BCT structure can be oriented to have a fully uncompensated interfacial spin plane (1 0 0) or a fully compensated interfacial spin plane (1 1 0) (shown in Fig. 2.6(a)). He included uniaxial anisotropy in the AFM crystal along the (0 0 1) axis, and the FM layer was modeled with no intrinsic anisotropy. Two different cases of the AFM interfacial spin plane are applied in the model: (1) a fully compensated interface and (2) a fully uncompensated interface. For both cases, he calculated the interfacial energy density as a function of the angle between the FM spins and the Neel axis of the AFM spins. The fully uncompensated interface gives the expected results of collinear coupling, a minimum at $\theta=0°$. However, the fully compensated interface gives the surprising result of an energy minimum at $\theta=90°$ indicating perpendicular interfacial coupling between the FM and AFM spins, shown in Fig. 2.6(b).

The Koon’s model is an important and interesting milestone in the development of a satisfactory understanding, and thus of a comprehensive theory of exchange anisotropy. It point out the importance of relative

orthogonal directions of the FM and AFM spins. However, contrary to Koon's expectation, spin flop coupling does not lead to the formation of a domain wall in the AFM during FM magnetization reversal and therefore in itself does not lead to exchange bias [22].

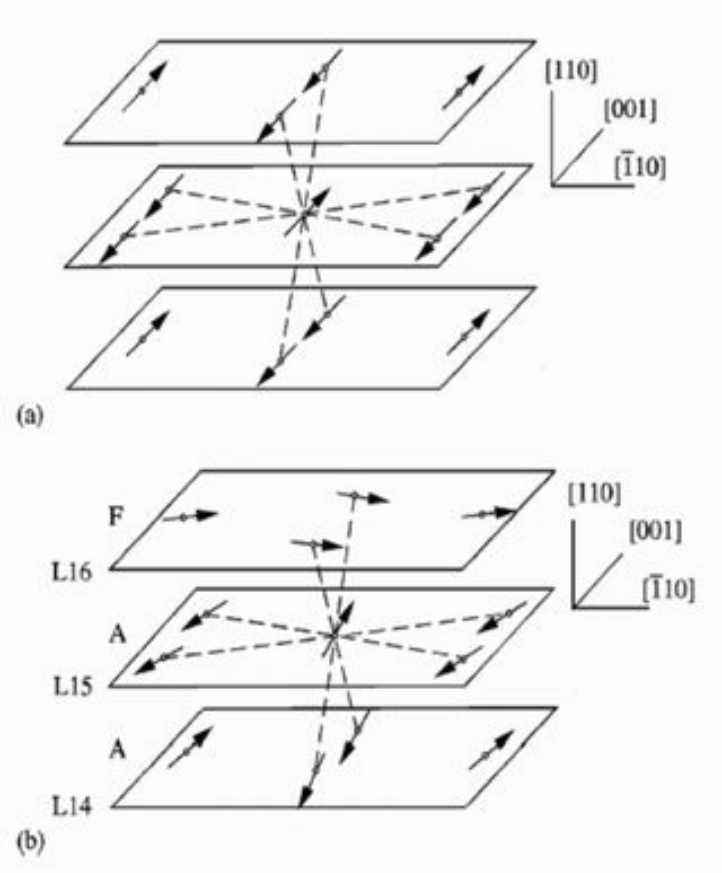

Fig. 2.6. (a) Magnetic structure of a body centered tetragonal (bct) AFM. (b) Lowest energy spin configuration near the interface plane. The interfacial AFM plane (L15) is fully compensated, and the interfacial FM plane (L16) is oriented perpendicular. The dashed lines represent the exchange bonds. (From Ref. [21])

2.1.c.5 Combine Defect Induced Random Field with Spin Flop Perpendicular Coupling(1999)

The work by Schulthess and Butler [22, 23] yielded findings contrary to Koon's calculations. They use an atomic Heisenberg model in conjuction with the classical Landau Lifshitz equation for the spin motion to study coupling mechanisms between FM and AFM. Considering the CoO with (111) interface planes as a model AFM-layer, and has a perpendicular alignment between the FM magnetization and AFM easy axis, which can be observed in many other FM/AFM system. Consequently, they have concluded that two coupling mechanisms, spin flop coupling and defect induced random fields, must be present. Their work yield the interfacial spin flopped state similar to Koon's, but had contrary conclusions with respect to exchange biasing. Their conclusion indicate that the enhanced uniaxial anisotropy or enhanced coercivity are caused by spin flop mechanism, but a shifted magnetization can not exist without the defect induced random field is present. On the other hand, if spin flop coupling were absent while the defect induced random field is present, the system would show exchange bias but neither no coupling induced coercivity nor perpendicular coupling.

2.1.c.6 Domain State Model(2002)

The domain state model proposed by Nowak, et al. [24, 25], explained the existence of the exchange bias effect through the interaction between nonmagnetic defects and the domain walls in the volume of the AFM and subsequent exchange coupling with the neighboring FM layer. The basis theory for the domain state model originated from the study of domain formation and interaction of these domains with defects in diluted Ising antiferromagnets in an external magnetic field [26]. According to these studies, it is energetically favorable for the walls of domains to pass through the nonmagnetic defects to reduce the energy for domain wall formation as shown in Fig. 2.7. The domain wall is represented by a solid line where the domain wall passes through the defects represented by the black dots. The magnetization of the individual atoms in the domain is represented by gray arrows. The domain has a total of three uncompensated spins, which leads to surplus magnetization in this part of the diluted antiferromagnet. This domain is surrounded by domains, represented by the black arrows, which have a net magnetization direction that is reversed with respect to the first domain. The domain state in the antiferromagnet can be oriented if the defects in the volume are created under an applied field or if the sample is cooled down below the T_b of the AFM while under an applied magnetic field. This leads to a net macroscopic magnetization in the volume of the AFM.

The situation becomes even more complex when a FM layer is deposited on top of a diluted Ising antiferromagnet as seen in Fig. 2.8. The domains in the AFM layer will now extend from the AFM/FM interface to the bottom of the AFM layer. The spins that are coupling within a domain are represented by the dashed lines. The uncompensated spins in the domain at the interface, Fig. 2.7, will couple with the spins of the neighboring atoms in the FM layer due to a interfacial energy difference. The coupling between the AFM and FM is represented by a solid line. A net surplus magnetization exists at the AFM/FM interface when the magnetization is averaged over a set number of domains. This leads to the observance of the exchange bias effect. Magnetic linear dichroism has been used to image the domains in both the FM and the AFM layer of AFM/FM bilayers to confirm this hypothesis [27]. The domains in both layers were found to coincide locally with one another an indication of exchange coupling across the AFM/FM interface

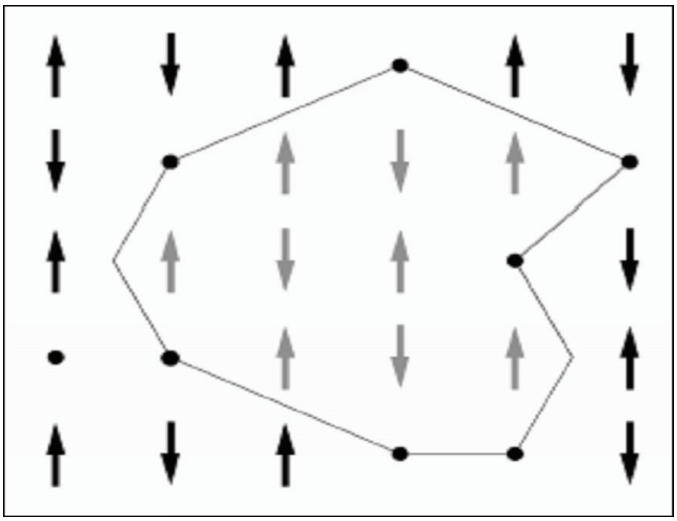

Fig. 2.7 Planar overview of diluted Ising antiferromagnet showing the role of defects in domain formation and the creation of uncompensated spins [25].

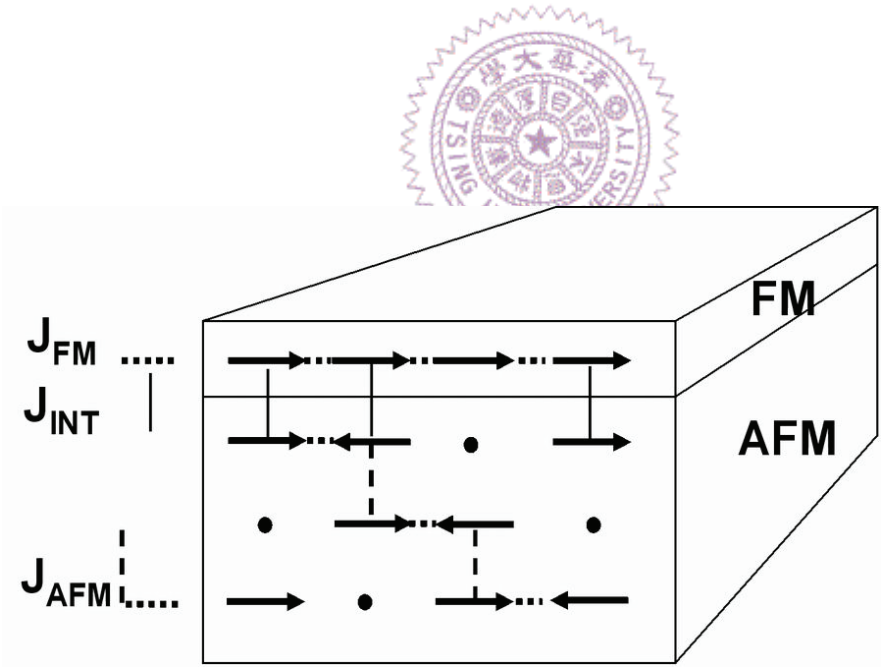

Fig. 2.8 Side view of AFM/FM bilayer illustrating the role of defects in domain formation in the volume of the AFM and the subsequent exchange coupling at the AFM/FM interface.

The defect density in the volume of the AFM determines the number of domain walls, the size of the surplus magnetization and the resulting magnitude of the exchange bias effect. The defects present at the AFM/FM interface, such as interface roughness, do not have any influence on the size of the exchange bias effect. The microstructure, which determines the defect density in the volume of the AFM, is the deciding factor that influences the strength of the exchange bias field. This model was confirmed experimentally by observing the change in H_{ex} as function of volume defect density in a CoO/Co bilayer grown by MBE [28]. Defects were introduced into the CoO AFM by changing the oxygen partial pressure during the deposition to allow for an excess or deficiency of oxygen in the CoO. The interface was protected from a change in defect density by the growth of 0.4 nm thick CoO layer at the interface Co/CoO. This was done prior to the substitution of the Mg for Co or increase in oxygen partial pressure. The Heb was found to increase to a maximum with increase in defect density and then decrease as the loss of longrange order in the crystal lattice destroyed the antiferromagnetic nature of the CoO layer. This model was also experimentally confirmed by the irradiation of NiFe/FeMn bilayers with the He+ ions [29]. The H_{eb} of the of NiFe/FeMn bilayers was found to also increase with the defect density in the AFM and subsequently disappear with further increase in defect density after the loss of long-order in the crystal lattice.

2.2 Exchange Coupling With Metallic AFM Films

2.2.a Introduction

Metallic antiferromagnetic materials have been of great importance due to its use in spin valve devices and magnetoresistive random access memory (MRAM). Although many investigations have been reported for exchange coupling with metallic AFM, there is actually less understanding of the basic phenomena when metallic AFM films are involved. There are several likely reasons for this situation. One of them is the spin structures are generally more complex in metallic AFM; i.e. multi-spin sublattices, and often vary with temperature or concentration. Another reason is the crystal structures of metallic AFMs often deviate more strongly from cubic symmetry than do the structures of the insulating AFMs. This makes it more difficult to grow suitable epitaxial fillms, whether bilayer or multilayer. Besides, the Neel temperatures (T_N) of the metallic AFMs are usually higher than for insulating AFMs. This means that it is not always possible to annealing from T_N without considering the structure changes such as grain growth and interdiffusion. Thus, it is not as convenient to work with model systems as with insulating AFM.

Among many kinds of metallic AFM materials, the Mn-based alloys; i.e. Mn-TM (TM is transition metal), with a high Neel temperature have been intensively investigated for application in magnetic recording devices which have been mention above. Especially, antiferromagnetic γ-IrMn disordered alloys have intensively been investigated for these devices

because of their high Neel temperature, excellent characteristics of the exchange coupling field and the corrosion resistance [30, 31]. In the following section, a detailed introduction of γ-IrMn disordered alloys system has been carried.

2.2.b γ-IrMn Properties

2.2.b.1 Lattice structure

There are the ordered and disordered states in the γ-phase Ir-Mn alloy system. The lattice constant and the Neel temperatures of γ-phase disordered Ir_XMn_{100-X} alloys were first investigated by Yamaoka [32]. He demonstrated that the Neel temperature of the disordered alloy around x=25 is very high, of about 730K among several kinds of Mn-based alloy systems. A recent study by Tomeno *et al.* [33] showed that $L1_2$-type ordered Mn_3Ir alloy also has a high Neel temperature of about 950 K. In previous studies, the exchange coupling field of γ-phase disordered Ir_XMn_{100-X} alloys increases abruptly with increasing Ir content from x=10 (H_{ex} is zero) to a sharp maximum value around x=20. On the contrary, they have a face-centered-tetragonal (fct) structure with the axial ratio $c/a>1$ from x=8 to 13 and the face-centered-cubic (fcc) structure up to x=31 [34]. Fig. 2.8 shows that all the fcc disordered γ-IrMn peaks are identified with x=29.4. With decreasing Ir concentration, the splitting of 200, 220 and 311 peaks in the diffraction pattern for the alloy with x=12.1, indicated the structure changes to a fct

structure with c>a. Furthermore, the split peak intensities change at x=7.6, showing the existence of an fco structure phase. However, the fco phase exist in a very narrow concentration range and β phase is more stable for lower Ir concentration, as shown at x=6.5, all the peaks are identified as a β Mn phase.

The phase diagram and lattice constants of the γ-phase disordered Ir_XMn_{100-X} alloy system is also shown in Fig. 2.9 and Fig.2.10, respectively, indicates the phase transformation temperature at room temperature from the face-centered-tetragonal (fct) to the face-centered-orthorhombic (fco) structure and from the face-centered-tetragonal (fct) to the face-centered-cubic (fcc) phase are given by T_0 and $T_{fct/fcc}$, respectively. Besides, the concentration dependence of T_N is obtained by the magnetic susceptibility measurement [35].

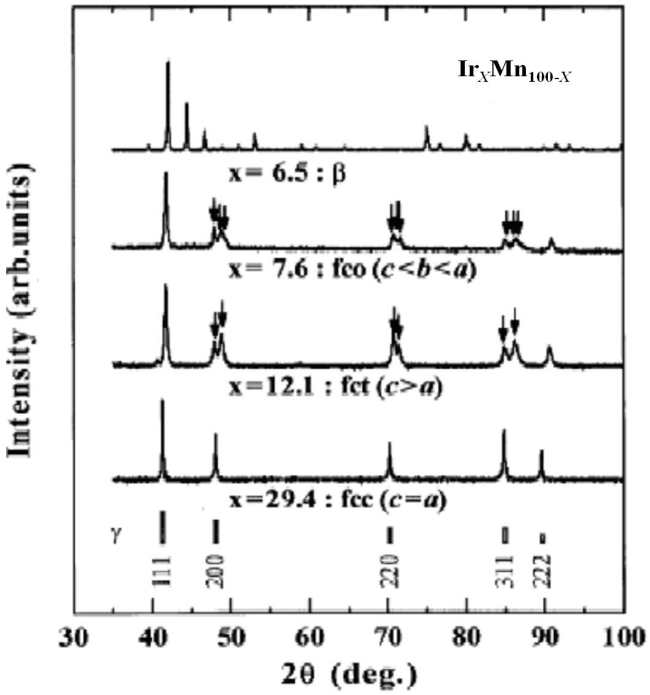

Fig. 2.9 The room temperature powder X-ray diffraction patterns of the γ-phase disordered Ir_XMn_{100-X} alloys, together with the calculated intensities at bottom for reference [35].

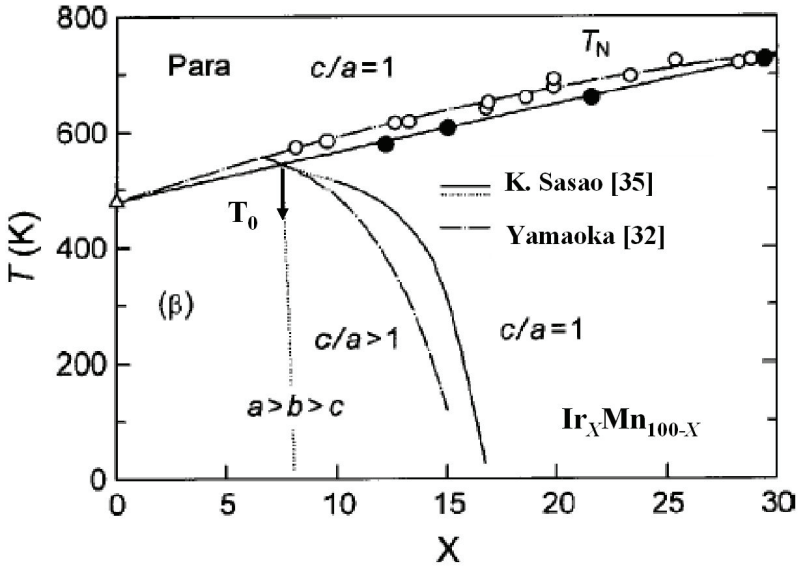

Fig. 2.10 Phase diagram of the γ-phase disordered Ir_XMn_{100-X} alloy system [35].

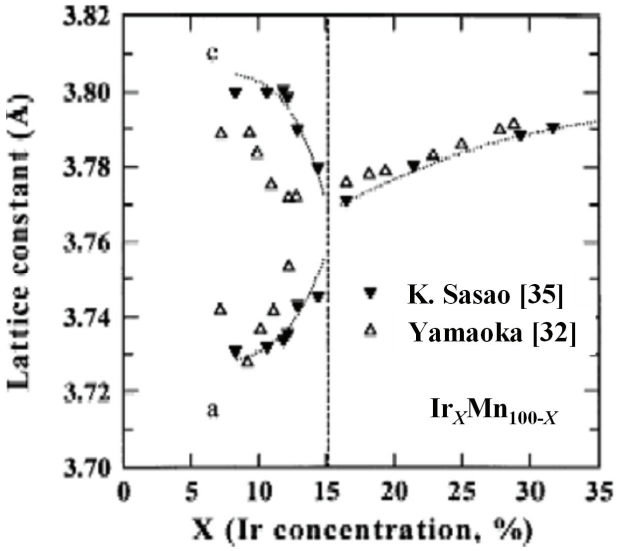

Fig. 2.11 The concentration dependence of the lattice constant of the γ-MnIr disordered alloys. [35]

2.2.b.2 Magnetic structure

Actually, the sequence of changes for the lattice distortion is similar in Mn-based alloys, that is, fcc, fct (***c>a***), fco and fct (***c<a***) structure changes take place with decreasing additive concentration. It has been reported in Mn-rich γ-MnFe [36], γ-MnNi [37], γ-MnRh[38], γ-MnPd [39], γ-MnPt [40] alloy systems stabilized about 20 at.% of additives. Since the exchange bias field properties have strong relation to the spin structures, it has been suggested that the spin structure changes together with the lattice distortions. Following the above description of lattice distortion, the magnetic structure changes in turn into single-Q (1Q), double-Q (2Q) and triple-Q (3Q) spin density wave (SDW) structure, which are generally called the multiple-Q SDW (MQSDW) structures [41], shown in Fig. 2.11(a)~(c). These spin structure changes have been experimentally been observed by neutron

diffraction [42], Mossbauer transmission spectra [43], and γ-ray emissions [44]. Recently, the first principles approach using the tight-binding linear muffin tin orbital (TB-LMTO) method, based on the local spin density (LSD) functional approximation, is used to calculated the electronic and the magnetic structure of **γ**-phase Ir_XMn_{100-X} alloys [45,46].

γ-phase disorder Ir_XMn_{100-X} alloys (0<x<30)

The magnetic structure of **γ**-phase disorder Ir_XMn_{100-X} alloys were first studied by Yomoka [47] in 1974, by using the neutron diffraction method, the **γ**-IrMn at room temperature has been characterized as the average spins on each (0 0 2) plane are aligned parallel along the *c*-axis with alternating signs on neighboring (0 0 2) planes; i.e. 1Q structure. The average moments per atom are 2.5 μ_B up to ~20 at% Ir, and drop to 0.8 μ_B at ~25.6 at% Ir. However, the recently reports using the first principles approach, which has been mentioned in the preceding subsection, have suggested that the 2Q or 3Q structures, which depends on variation of concentration, is the most stable in the **γ**-phase disorder IrMn alloys. For the discrepancy between the spin structures, one may notice that powder neutron diffractions are unable to distinguish between the 1Q and the 3Q structure.

To investigate the concentration dependence of magnetic structures, it has been reported that in room temperature of pure **γ**-Mn (x=0), the 2Q structure is the most stable state among the MQSDW structures. However, the total energy of 3Q decreasing as the concentration of Ir increasing and becomes the most stable state around x=13. and remains the most stable state with further increasing of x, seen in Fig. 2.12. Notice that the Ir concentration where the magnetic transition from the 2Q to the 3Q structure takes place is

quite close to the concentration at which the axial ratio changes from c/a>1 to c/a=1. Actually, from the calculation, it has been inferred that the critical concentration defined by x_m for the magnetic transition is put forward to a higher concentration by a few percent if the lattice distortion takes place [46].

$L1_2$ type ordered phase of Mn_3Ir alloys

The $L1_2$ type ordered phase Mn_3Ir alloys, which provided a large exchange anisotropy constant (J_K is up to 1.3erg/cm^3) and high blocking temperature (T_b) had been reported by M. Takahashi in 2004 [48,49]. The magnetic structure of Mn_3Ir in Fig. 2.11(d) represents a triangular (T1) structure, which was proposed by Kouvel and Kasper [50] and Kren et al.[40] for ordered Mn_3Rh and Mn_3Pt alloys. The Mn moments are parallel to the (111) plane and aligned in the <112> direction. The magnetic structure of the $L1_2$-type ordered Mn_3Ir has been identified as the same [33]. The ordered phase Mn_3Ir alloys can be experimentally obtained by thermal annealing after the disordered γ-$Ir_{25}Mn_{75}$ alloy is deposited at room temperature [51].

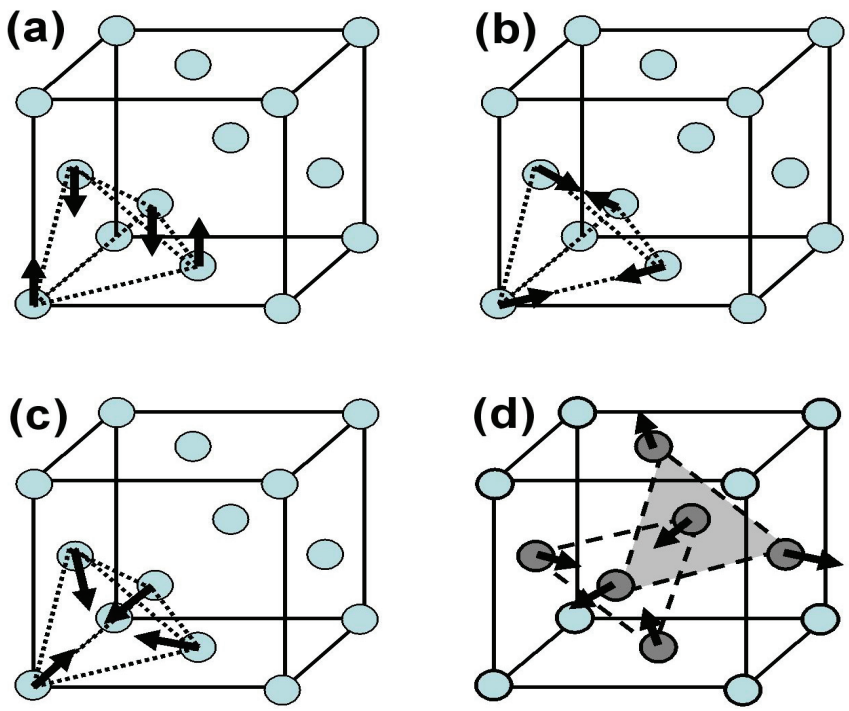

Fig. 2.12 Spin structure of γ-phase IrMn alloys. (a) 1Q, (b) 2Q, and (c) 3Q structure in the disordered fcc lattice. (d) $L1_2$ ordered phase of Mn_3Ir alloys.

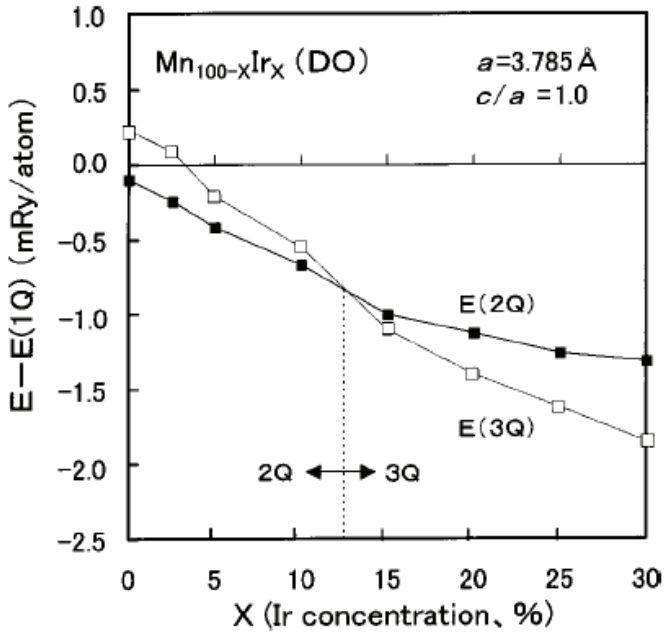

Fig. 2.13 Concentration dependence of the electronic total energyof the g-phase disordered (DO) Ir_xMn_{100-x} alloys for the 2Q and the 3Q structures. The total energy is given relative to that of the 1Q structure.

2.2.b.3 Influence of the spin structure on exchange bias of FM/AFM

The models of exchange anisotropy mentioned in section 2.1 are based on a collinear spin structure in the AFM layer, which shows an antiparallel arrangement of AFM spins. However, it should be emphasized that the spin structure for several kinds of γ-phase disordered alloys are not collinear; i.e. 3Q or T1 structure. Recently, the quantitative explanation for the influence of non-collinear spin structure is given by C. Mitsumata *et al.* [52,53]. In

their works, the framework of the classical Heisenberg model is used. In order to define the magnetic structure in FM/AFM bilayer, the following Hamiltonian described in equation listed below is evaluated in the numerical calculations.

$$H = -\sum_{\langle i,j \rangle} J_{1ij}\boldsymbol{S}_i \cdot \boldsymbol{S}_j - \sum_{\langle i,k \rangle} J_{2ik}\boldsymbol{S}_i \cdot \boldsymbol{S}_k - \sum_i D_i(\boldsymbol{S}_i \cdot \boldsymbol{n})^2 - g\mu_{\mathrm{B}} \sum_i \boldsymbol{S}_i \cdot \boldsymbol{H}.$$

The unit vector $\boldsymbol{S_i}$ denotes the spin at the ***i***th atom, and the summation is carried out over all possible spin pairs by using the exchange constants $\boldsymbol{J_1}$ and $\boldsymbol{J_2}$. The third and fourth terms in equation describe the magnetic anisotropy energy and Zeeman energy, respectively. Here, and unit vector mean the anisotropy constant and the direction of an easy axis, and the vector represents the applied field. Their discussion focus on the <111> stacking of the FM/AFM bilayers, which has the 3Q magnetic structure in AFM. For the AFM spins, four equivalent atoms are composed in the unit cell, and the summation of those spins should become zero in the ground state, which leads to a fully compensated <111> surface. In this case, it should not be observed any exchange bias phenomenon at the <111> FM/AFM interface. However, the exchange bias is actually observed in <111> stacked bilayers. The contradiction was explained by the frustrated spins at the interface of FM/AFM, seen in the Fig illustrated the 3Q FM/AFM interface, one can see that the direction of the AFM spin near the interface is different from that of the ground state. The relaxation of spins influences the deviation of angles between the AFM spins. Consequently, the

resultant spin element becomes finite, forming the uncompensated spins in the AFM layer. Such uncompensated spin element is quite small, but can be observed by X-ray magnetic circular dichroism (XMCD) spectroscopy [54,55].

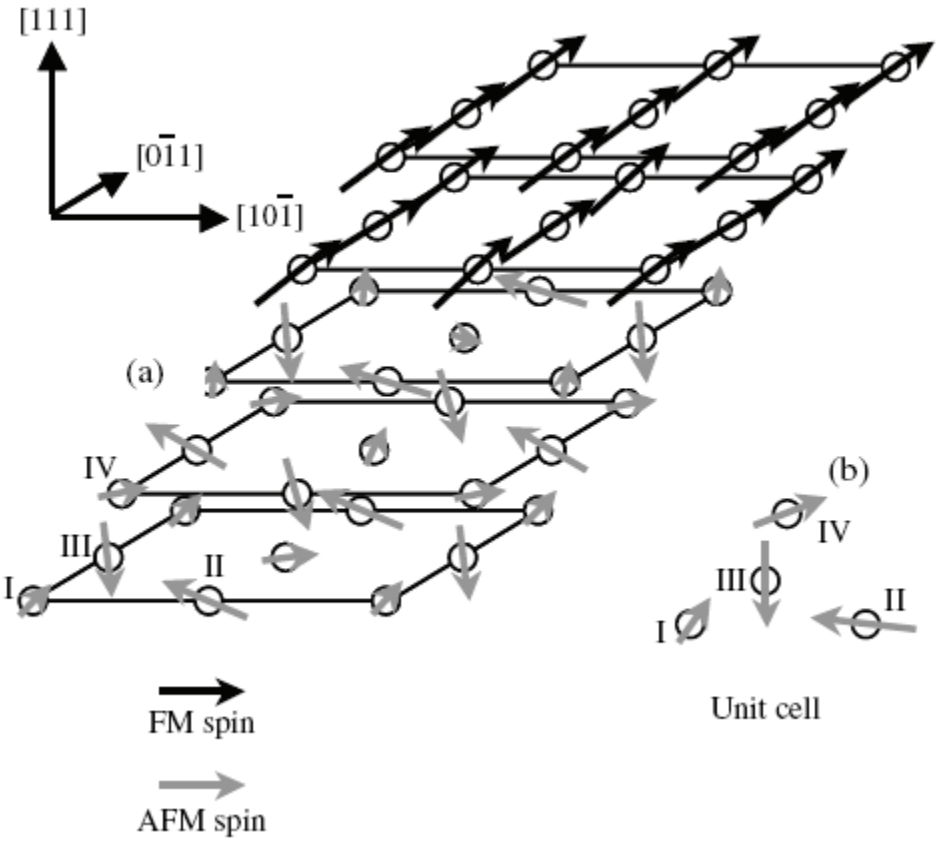

Fig. 2.14 The spin configuration of the AFM/FM bilayer. (a) The spin configuration near the interface, (b) the ground state of the spin structure in the magnetic unit cell.